Publisher: GSA
Journal: GEOL: Geology
DOI:10.1130/G37529.1

Is the Troodos ophiolite (Cyprus) a complete, transform fault–bounded Neotethyan ridge segment?

Antony Morris[1] and Marco Maffione[2]

[1]*School of Geography, Earth and Environmental Sciences, Plymouth University, Drake Circus, PL4 8AA Plymouth, UK*

[2]*Department of Earth Sciences, Utrecht University, Heidelberglaan 2, 3584 CS Utrecht, Netherlands*

ABSTRACT

We report new paleomagnetic data from the sheeted dike complex of the Troodos ophiolite (Cyprus) that indicate a hitherto unrecognized oceanic transform fault system marks its northern limit. The style, magnitude and scale of upper crustal fault block rotations in the northwestern Troodos region mirror those observed adjacent to the well-known Southern Troodos Transform Fault Zone along the southern edge of the ophiolite. A pattern of increasing clockwise rotation toward the north, coupled with consistent original dike strikes and inclined net rotation axes across this region, is compatible with distributed deformation adjacent to a dextrally slipping transform system with a principal displacement zone just to the north of the exposed ophiolite. Combined with existing constraints on the spreading fabric, this implies segmentation of the Troodos ridge system on length scales of ~40 km, and suggests that a coherent strip of Neotethyan lithosphere, representing a complete ridge segment bounded by transforms, has been uplifted to form the currently exposed Troodos ophiolite. Moreover, the inferred length scale of the ridge segment is consistent with formation at a slow-spreading rate during Tethyan seafloor

spreading and with a supra-subduction zone environment, as indicated by geochemical constraints.

INTRODUCTION

The Troodos Complex of Cyprus is one of the world's best preserved ophiolites (Gass, 1968; Moores and Vine, 1971). It formed during the Late Cretaceous (Cenomanian–Turonian, U–Pb age 90–92 Ma; Mukasa and Ludden 1987) at a supra-subduction zone spreading axis within the Neotethyan Ocean (Pearce, 2003), and consists of a complete Penrose pseudostratigraphy disposed in a domal structure as a result of focused Late Pliocene–Recent uplift (Robertson, 1990). Previous paleomagnetic and structural analyses, focused on central and eastern Troodos (Clube and Robertson, 1986; Bonhommet et al., 1988; Allerton, 1989a; MacLeod et al., 1990; Morris et al., 1990), identified preservation of a fossil oceanic spreading ridge-transform fault system, allowing models of transform tectonics to be developed and tested (Allerton, 1989b; MacLeod et al., 1990; Gass et al., 1991). This Southern Troodos Transform Fault Zone (STTFZ) (MacLeod and Murton, 1993) is characterized by differential clockwise rotations around inclined axes of small (≤1 km), upper crustal fault blocks adjacent to a dextrally-slipping transform, active during Late Cretaceous seafloor spreading (Clube and Robertson, 1986; Bonhommet et al., 1988; Allerton, 1989a; MacLeod et al., 1990; Morris et al., 1990; Scott et al., 2013; Cooke et al., 2014). Variable, shearing-induced rotations resulted in tectonic disruption of the trend of sheeted dikes that originally intruded with a consistent NW-SE strike (present-day coordinates; Allerton and Vine, 1987; Allerton, 1989a). The western limit of these distributed, localized rotations along the STTFZ defines a fossil ridge-transform intersection (MacLeod et al., 1990) that aligns with the inferred main spreading axis of the Solea graben (Hurst et al., 1992) to the north.

Here we present an analysis of net tectonic rotations in sheeted dikes to the west of the Solea axis, a region representing ~40% of the total spreading-parallel width of the exposed sheeted dike complex but where no previous systematic studies have been undertaken. Dikes in this region also have variable present-day orientations suggesting significant fault block rotations. Paleomagnetic analysis using a net tectonic rotation approach allows determination of the initial strike of these dikes and assessment of the pattern of tectonic rotations, providing new information on the spreading structure and significance of this paleomagnetically unexplored part of the ophiolite.

DIKE ORIENTATIONS, SAMPLING AND PALEOMAGNETIC DATA

Surprisingly, given decades of international interest in the tectonic evolution of Troodos, the sheeted dike complex of the northwestern domain of the ophiolite has received only minor attention, with limited mapping of dike trends or fault zones (Cooke et al., 2014) and paleomagnetic data only reported previously from two isolated sites (Morris et al., 1998). However, road-cut sections offer near-continuous exposure of sheeted dikes, which have been shown elsewhere in the ophiolite to carry stable, early, seafloor spreading-related magnetic remanences (e.g., Allerton and Vine, 1987; Bonhommet et al., 1988; Hurst et al., 1992) that pre-date deformation (Morris, 2003; Morris et al., 2006) and may therefore be used as markers for tectonic rotation.

Field structural analysis from an ~30 km transect along the Pachyammos-Stavros tis Psokas-Lysos road in the western Troodos (Fig. 1) reveals distinct differences in dike orientation as the northern edge of the exposed ophiolite is approached: a southern domain with generally N-S–striking dikes (mean strike/dip = 173°/53°; α_{95} = 7.4°) changes northward to a domain with ENE-WSW–striking dikes (mean strike/dip = 237°/48°; α_{95} = 10.4°) (Fig. DR1 in the GSA Data Repository[1]).

Paleomagnetic samples were collected along this transect at 23 sites in sheeted dikes. At each site, eight to ten oriented cores were drilled from adjacent dikes with consistent orientation, one core per dike, to maximize averaging of secular variation. Mean dike orientations and associated errors (α_{95}) at each site were obtained by averaging structural measurements from each sampled dike. At five sites (WT03, WT05, WT09, WT12, and WT14), single, discrete dikes were observed to obliquely cut across the sheeted sequences. These were sampled separately (sites WT04, WT06, WT10, WT13, and WT15) but proved to have magnetization directions identical to the host sheeted dikes (Table DR1 in the Data Repository). They demonstrably were not emplaced vertically and hence cannot be used in tectonic analyses. The in situ remanences from all sites are reported (Table DR1), but only results from sheeted dikes are discussed hereafter.

Standard paleomagnetic laboratory analyses (see the Data Repository) yielded statistically well-defined site magnetization vectors (SMVs; Table DR1), after removal of minor low stability viscous overprints (Fig. DR2a). Paleosecular variation of the geomagnetic field is well-represented at 20 sites, according to the criteria of Deenen et al. (2011) ($A_{95min} < A_{95} < A_{95max}$; Table DR1), supporting a primary origin of the remanence. At the remaining three sites (WT18, WT19, WT20) paleosecular variation is under-represented (i.e., $A_{95} < A_{95min}$), probably due to rapid, near-simultaneous acquisition of thermoremanent magnetization by sampled dikes.

The Troodos ophiolite experienced bulk ~90° counterclockwise rotation as an oceanic microplate after cessation of seafloor spreading (Clube and Robertson, 1986; Morris et al., 1990). West-directed remanences of upper crustal units away from zones of localized deformation (i.e., away from the STTFZ) reflect this plate-scale rotation (Moores and Vine, 1971; Clube et al., 1985; Morris et al., 2006) and define the so-called 'Troodos magnetization vector' reference direction (TMV; declination/inclination = 274°/36°, α_{95} = 7.0°; Clube and Robertson, 1986). SMVs from the majority of sites show consistent WNW directions with shallow-moderate inclinations that are statistically different to the TMV (Fig. DR2b), demonstrating localized rotations of these units. Exceptions are sites WT09 and WT26 where SMVs are statistically indistinguishable from the TMV (Table DR1). However, moderate dips of dikes at these sites indicate that some deformation has occurred.

NET TECTONIC ROTATION ANALYSIS

Paleomagnetic data are commonly interpreted tectonically by rotating sampled units (and associated remanence vectors) to a local paleohorizontal or paleovertical around present-day, strike-parallel axes. Such standard tilt corrections arbitrarily divide the total deformation at a site into a vertical axis rotation followed by a tilt. This approach is inadequate in sheeted dike terrains where components of rotation around dike-normal axes do not result in observable changes in dike orientation (Borradaile, 2001; Morris and Anderson, 2002). In these settings, it is more appropriate to calculate the single net tectonic rotation around an inclined axis at a site that restores the SMV to an appropriate reference direction and observed dike margins back to the paleovertical.

Here we apply an algorithm devised by Allerton and Vine (1987), and subsequently applied in Troodos and other ophiolites (Allerton, 1989a; Morris et al., 1990, 1998; Morris and Anderson, 2002; Hurst et al., 1992; Inwood et al., 2009), that yields the azimuth and plunge of the net rotation axis, the magnitude and sense of rotation, and the initial dike orientation (see the Data Repository). Following previous studies (e.g., Allerton and Vine, 1987; Allerton, 1989a; Morris et al., 1998), we use the TMV as a reference direction, representing the regional magnetization direction of the Troodos ophiolite after microplate rotation. Hence, dikes are restored to primary orientations that exclude the effects of microplate rotation, allowing comparison with elements of the Troodos spreading structure established in the current geographic reference frame.

Net tectonic rotation analysis at all sites yield two solutions capable of restoring dikes to the paleovertical (Table DR2). Solutions providing NW-SE initial dike strikes show systematic clockwise rotations (looking in the direction of the rotation pole azimuth) and comparable orientations of rotation axes (Fig. 1; Fig. DR3; Table DR2). Alternate solutions giving E-W or NE-SW initial dike strikes yield variable senses of rotation (Table DR2), which are unlikely. Moreover, solutions yielding NW-SE strikes have been accepted in previous studies (Allerton, 1989a; Morris et al., 1998) in areas of the ophiolite where it was possible to show that alternate solutions restored associated lavas to geological implausible initial orientations. NW-SE–striking solutions have been chosen, therefore, as preferred solutions in this study (Table DR2). Permissible rotation poles are well-clustered at most sites (Fig. DR4), indicating that calculated net tectonic rotation solutions based on mean input vectors are reliable and can be used for tectonic interpretation. Conversely, four sites (WT11, WT12, WT14, and WT26) showing larger scatter of permissible rotation poles (Fig. DR4; Table DR2) have been discarded from further analyses.

While rotation poles have comparable orientations across the study area, rotation magnitudes are highly variable (Fig. 1; Table DR2; Fig. DR5) and fall into two broad domains (Fig. 1; Fig. DR3): a northern area containing seven sites characterized by very large (>90°) rotations, and a southern area containing 12 sites characterized by moderate (<80°) rotations. Overall, net rotation magnitudes progressively decrease southward with a rapid change in the first ~10 km from the northern edge of the study area. Importantly, consistent initial dike orientations are found for all sites (Fig. 1, inset), despite highly variable present-day orientations (Fig. DR1). This demonstrates that dikes were emplaced with common NW-SE strikes (relative to present-day north) and were subsequently disrupted by variable tectonic rotations of fault blocks. The absence of any major faults in this region suggests that deformation was distributed, with rotations likely to be accommodated by displacement on minor faults (Peacock et al., 1998).

COMPARISON WITH THE SOUTHERN TROODOS TRANSFORM FAULT ZONE

The characteristics of rotational deformation in the study area (common initial dike orientations, rotation around inclined axes, and progressive change in rotation magnitude from north to south) are remarkably similar to those documented previously in the region adjacent to the STTFZ. Dikes to the east of the Solea graben progressively swing from NNW-SSE through NE-SW to ENE-WSW strikes across an ~10-km-wide zone of distributed deformation as the STTFZ is approached (Fig. 1). This reflects systematically clockwise but variable local rotations of initially NW-SE striking dikes (relative to present-day north) during dextral slip along the transform (Clube and Robertson, 1986; Bonhommet et al., 1988; Allerton, 1989a; MacLeod et al., 1990; Scott et al., 2013). No major faults exist within this zone of rotation north of the STTFZ, again indicating distributed deformation. Dikes within our study area mirror this pattern on a similar length scale, with NW-SE initial emplacement and subsequent rotations resulting in a marked variation in present-day orientations (from N-S to ENE-WSW strikes moving northward), but in this case, with the largest rotations recorded in the northernmost sites.

DISCUSSION

The evidence for consistent clockwise rotations of sheeted dikes around inclined axes with systematic variations in rotation magnitude from north to south across the study area precisely matches the style and scale of transform-related deformation observed in the STTFZ. The rotations observed in NW Troodos cannot be attributed to post-seafloor spreading tectonics. The dominant neotectonic structure in this region is the Polis graben to the west of the study area, which formed in the Miocene by ENE-WSW extension, driven by subduction roll-back and trench migration (Payne and Robertson, 1995). Structures associated with this event are not observed in the study area and, in any case, could only account for minor tilting. The most significant earlier post-spreading tectonic event affecting the ophiolite was paleorotation of the Troodos microplate, which initiated in the Late Cretaceous and ended in the Eocene (Moores and Vine, 1971; Clube and Robertson, 1986). A post-accretion phase of stretching related to this event has been documented in the eastern part of the Limassol Forest Complex, within the STTFZ (MacLeod, 1990). This led to development of a low angle extensional detachment fault system (the Akapnou Forest Décollement; MacLeod, 1990) which was founded upon, and reused, earlier transform-related structures. However, there is no evidence for post-spreading extensional structures in NW Troodos, and, although their location is uncertain, microplate boundaries must lie to the W of the Akamas peninsula (Fig. 1), which demonstrably rotated as part of the microplate (Clube and Robertson, 1986; Morris et al., 1998).

We propose, therefore, that clockwise tectonic rotations in NW Troodos are instead related to distributed deformation adjacent to a dextrally slipping "Northern Troodos Transform Fault Zone" (NTTFZ), with a principal displacement zone located just to the N of the exposed ophiolite (Fig. 2). Clockwise rotations around inclined axes plunging to the NW are likely due to the combined effects of rotation induced by shear along the transform and tilting during seafloor spreading–related extension. This latter component may reflect off-axis amagmatic extension, as inferred by Cooke et al. (2014) from a structural analysis of the north Troodos margin just to the east of our study area. We suggest an E-W trend for the NTTFZ, parallel to the Arakapas Fault. A WNW-ESE strike parallel to the northern margin of the exposed ophiolite is precluded by net tectonic rotation data from dikes in the Solea graben (Hurst et al., 1992) that show simple tilting around horizontal axes and no evidence for a transform influence.

Together, the NTTFZ and STTFZ delineate the limits of an ~40-km-long Solea spreading segment. This suggests that the Troodos spreading system was characterized by short segments with transform offsets of similar or longer length-scale. This model (Fig. 2A) can also explain the presence of extrusive rocks in the northern Akamas peninsula that have geochemical signatures similar to transform active sequences in the STTFZ

(Murton, 1990), an observation that is difficult to account for if the STTFZ represents the only oceanic transform system preserved in the Troodos ophiolite (Morris et al., 1998). This spreading geometry can account for the pronounced E-W elongation of the exposed Troodos ophiolite, as it suggests that major transform/fracture zone structures mark both its northern and southern limits.

The length scale of the Solea spreading segment, bounded by the NTTFZ and STTFZ, is similar to that observed in several modern supra-subduction zone systems (for example, in the Andaman Sea (Fig. 2B), the Manus Basin, and the East Scotia Ridge; Moores et al., 1984; Davies, 2012; Barker, 2001). This is consistent with geochemical evidence (e.g., Pearce, 2003) that indicates formation of the Troodos ophiolite in a supra-subduction zone environment, and supports an earlier suggestion by Moores et al. (1984) that the Troodos system was likely marked by short ridge segments. Finally, there have been considerable differences in estimates of the spreading rate of the Troodos ridge system, from slow (Abelson et al., 2001) to intermediate-fast spreading (e.g., Allerton and Vine, 1987, 1990). A first-order constraint on this is provided by a systematic (but nonlinear) relationship between segment length and spreading rate (Sandwell 1986; Sandwell and Smith, 2009). Using this relationship, the length-scale of the Solea segment indicates that the Troodos ophiolite formed by spreading at a slow rate (of <4 cm/year, full rate).

ACKNOWLEDGMENTS

We thank Chun-Tak Chu for assistance in the field and for undertaking some of the laboratory analyses, and Sarah Titus and an anonymous referee for helpful reviews. Stereonets were produced using OSXStereonet (Cardozo and Allmendinger, 2013).

REFERENCES CITED

Abelson, M., Baer, G., and Agnon, A., 2001, Evidence from gabbro of the Troodos ophiolite for lateral magma transport along a slow-spreading mid-ocean ridge: Nature, v. 409, p. 72–75, doi:10.1038/35051058.

Allerton, S., 1989a, Fault block rotations in ophiolites: Results of palaeomagnetic studies in the Troodos Complex, Cyprus, *in* Kissel, C., and Laj, C., eds., Palaeomagnetic Rotations and Continental Deformation: NATO ASI Series C, v. 254, p. 393–410, doi:10.1007/978-94-009-0869-7_24.

Allerton, S., 1989b, Distortions, rotations and crustal thinning at ridge-transform intersections: Nature, v. 340, p. 626–628, doi:10.1038/340626a0.

Allerton, S., and Vine, F.J., 1987, Spreading structure of the Troodos ophiolite, Cyprus: Some paleomagnetic constraints: Geology, v. 15, p. 593, doi:10.1130/0091-7613(1987)15<593:SSOTTO>2.0.CO;2.

Allerton, S., and Vine, F.J., 1990, Palaeomagnetic and structural studies of the southeastern part of the Troodos complex, *in* Malpas, J., et al., eds., Ophiolites: Oceanic Crustal Analogues: Proceedings of the symposium "Troodos 1987", Ministry of Agriculture and Natural Resources, Geological Survey Department, Republic of Cyprus, Nicosia, Cyprus, p. 99–111.

Barker, P.F., 2001, Scotia sea regional tectonic evolution: Implications for mantle flow and palaeocirculation: Earth-Science Reviews, v. 55, p. 1–39, doi:10.1016/S0012-8252(01)00055-1.

Bonhommet, N., Roperch, P., and Calza, F., 1988, Paleomagnetic arguments for block rotations along the Arakapas fault (Cyprus): Geology, v. 16, p. 422, doi:10.1130/0091-7613(1988)016<0422:PAFBRA>2.3.CO;2.

Borradaile, G.J., 2001, Paleomagnetic vectors and tilted dikes: Tectonophysics, v. 333, p. 417–426, doi:10.1016/S0040-1951(00)00296-1.

Cardozo, N., and Allmendinger, R.W., 2013, Spherical projections with OSXStereonet: Computers & Geosciences, v. 51, p. 193–205, doi:10.1016/j.cageo.2012.07.021.

Clube, T.M.M., and Robertson, A.H.F., 1986, The palaeorotation of the Troodos microplate, Cyprus, in the late Mesozoic-early Cenozoic plate tectonic framework of the Eastern Mediterranean: Surveys in Geophysics, v. 8, p. 375–437, doi:10.1007/BF01903949.

Clube, T.M.M., Creer, K.M., and Robertson, A.H.F., 1985, Palaeorotation of the Troodos microplate, Cyprus: Nature, v. 317, p. 522–525, doi:10.1038/317522a0.

Cooke, A.J., Masson, L.P., and Robertson, A.H.F., 2014, Construction of a sheeted dyke complex: evidence from the northern margin of the Troodos ophiolite and its southern margin adjacent to the Arakapas fault zone: Ofioliti, v. 39, p. 1–30, doi:10.4454/ofioliti.v39i1.426.

Davies, H.L., 2012, The geology of New Guinea -the cordilleran margin of the Australian continent: Episodes, v. 35, p. 87–102.

Deenen, M.H.L., Langereis, C.G., van Hinsbergen, D.J.J., and Biggin, A.J., 2011, Geomagnetic secular variation and the statistics of palaeomagnetic directions: Geophysical Journal International, v. 186, p. 509–520, doi:10.1111/j.1365-246X.2011.05050.x.

Gass, I.G., 1968, Is the Troodos massif of Cyprus a fragment of Mesozoic ocean floor?: Nature, v. 220, p. 39–42, doi:10.1038/220039a0.

Gass, I.G., MacLeod, C.J., Murton, B.J., Panayiotou, A., Simonian, K.O., and Xenophontos, C., 1991, Geological Map of the South Troodos Transform Fault Zone at 1:25.000: Sheets 1 (west) and 2 (east): Nicosia, Cyprus Geological Survey Department.

Hurst, S.D., Verosub, K.L., and Moores, E.M., 1992, Paleomagnetic constraints on the formation of the Solea graben, Troodos ophiolite: Tectonophysics, v. 208, p. 431–445, doi:10.1016/0040-1951(92)90439-D.

Inwood, J., Morris, A., Anderson, M.W., and Robertson, A.H.F., 2009, Neotethyan intraoceanic microplate rotation and variations in spreading axis orientation: Palaeomagnetic evidence from the Hatay ophiolite (southern Turkey): Earth and Planetary Science Letters, v. 280, p. 105–117, doi:10.1016/j.epsl.2009.01.021.

MacLeod, C.J., 1990, Role of the Southern Troodos Transform Fault in the rotation of the Cyprus microplate: Evidence from the Eastern Limassol Forest, *in* Malpas, J., Moores, E.M., Panayiotou, A., and Xenophontos, C., eds., Ophiolites: Oceanic Crustal Analogues: Nicosia, Cyprus Geological Survey Department, p. 75–85.

MacLeod, C.J., and Murton, B.J., 1993, Structure and tectonic evolution of the Southern Troodos Transform Fault Zone, Cyprus, *in* Prichard, H.M., et al., eds., Magmatic Processes and Plate Tectonics: Geological Society, London, Special Publication 76, p. 141–176, doi:10.1144/GSL.SP.1993.076.01.07.

MacLeod, C.J., Allerton, S., Gass, I.G., and Xenophontos, C., 1990, Structure of a fossil ridge-transform intersection in the Troodos ophiolite: Nature, v. 348, p. 717–720, doi:10.1038/348717a0.

Moores, E.M., and Vine, F.J., 1971, The Troodos Massif, Cyprus and other ophiolites as oceanic crust: Evaluation and implications: Philosophical Transactions of the Royal Society of London, v. 268, p. 443–467, doi:10.1098/rsta.1971.0006.

Moores, E.M., Robinson, P.T., Malpas, J., and Xenophontos, C., 1984, Model for the origin of the Troodos massif, Cyprus, and other mideast ophiolites: Geology, v. 12, p. 500–503, doi:10.1130/0091-7613(1984)12<500:MFTOOT>2.0.CO;2.

Morris, A., 2003, The Late Cretaceous palaeolatitude of the Neotethyan spreading axis in the eastern Mediterranean region: Tectonophysics, v. 377, p. 157–178, doi:10.1016/j.tecto.2003.08.016.

Morris, A., and Anderson, M.W., 2002, Palaeomagnetic results from the Baër-Bassit ophiolite of northern Syria and their implication for fold tests in sheeted dyke terrains: Physics and Chemistry of the Earth, v. 27, p. 1215–1222, doi:10.1016/S1474-7065(02)00123-7.

Morris, A., Creer, K.M., and Robertson, A.H.F., 1990, Palaeomagnetic evidence for clockwise rotations related to dextral shear along the Southern Troodos Transform Fault, Cyprus: Earth and Planetary Science Letters, v. 99, p. 250–262, doi:10.1016/0012-821X(90)90114-D.

Morris, A., Anderson, M.W., and Robertson, A.H.F., 1998, Multiple tectonic rotations and transform tectonism in an intraoceanic suture zone, SW Cyprus: Tectonophysics, v. 299, p. 229–253, doi:10.1016/S0040-1951(98)00207-8.

Morris, A., Anderson, M.W., Inwood, J., and Robertson, A.H.F., 2006, Palaeomagnetic insights into the evolution of Neotethyan oceanic crust in the eastern Mediterranean: Geological Society of London, Special Publications, v. 260, p. 351–372, doi:10.1144/GSL.SP.2006.260.01.15.

Mukasa, S.B., and Ludden, J.N., 1987, Uranium-lead isotopic ages of plagiogranites from the Troodos ophiolite, Cyprus, and their tectonic significance: Geology, v. 15, p. 825, doi:10.1130/0091-7613(1987)15<825:UIAOPF>2.0.CO;2.

Murton, B.J., 1990, Was the Southern Troodos Transform Fault a victim of microplate rotation? *in* Malpas, J., et al., eds., Ophiolites: Oceanic Crustal Analogues: Nicosia, Cyprus Geological Survey Department, p. 87–98.

Payne, A.S., and Robertson, A.H.F., 1995, Neogene supra-subduction zone extension in the Polis graben system, west Cyprus: Journal of the Geological Society, v. 152, p. 613-628.

Peacock, D.C.P., Anderson, M.W., Morris, A., and Randall, D.E., 1998, Evidence for the importance of ‘small’ faults on block rotation: Tectonophysics, v. 299, p. 1–13, doi:10.1016/S0040-1951(98)00195-4.

Pearce, J.A., 2003, Supra-subduction zone ophiolites: The search for modern analogues, *in* Dilek, Y., and Newcomb, S., eds., Ophiolite Concept and the Evolution of Geological Thought: Geological Society of America Special Paper 373, p. 269–293, doi:10.1130/0-8137-2373-6.269.

Robertson, A.H.F., 1990, Tectonic evolution of Cyprus, *in* Malpas, J., et al., eds., Ophiolites: Oceanic Crustal Analogues: Nicosia, Cyprus Geological Survey Department, p. 235–252.

Sandwell, D.T., 1986, Thermal stress and the spacing of transform faults: Journal of Geophysical Research, v. 91, p. 6405–6417, doi:10.1029/JB091iB06p06405.

Sandwell, D.T., and Smith, W.H.F., 2009, Global marine gravity from retracked Geosat and ERS-1 altimetry: Ridge segmentation versus spreading rate: Journal of Geophysical Research. Solid Earth, v. 114, B01411, doi:10.1029/2008JB006008.

Scott, C.P., Titus, S.J., and Davis, J.R., 2013, Using field data to constrain a numerical kinematic model for ridge-transform deformation in the Troodos ophiolite, Cyprus: Lithosphere, v. 5, p. 109–127, doi:10.1130/L237.1.

FIGURE CAPTIONS

Figure 1. Geological map of the Troodos ophiolite (Cyprus) showing the location of the study area, and main structural features, such as the axis and edges of the Solea graben (red lines), the Southern Troodos Transform Fault Zone (STTFZ), and the general orientation of sheeted dikes (short black lines). The region in the study area characterized by the most highly rotated dikes (north domain; see text) is shaded in gray. Inset: results of net tectonic rotation analysis for the northern and southern domains of the study area, shown as rose diagrams of initial dike orientations (left), contoured equal area stereographic projections of permissible rotation axes (center), and frequency distributions of rotation magnitudes (right).

Figure 2. A: Proposed tectonic model for the origin of clockwise fault block rotations in NW Troodos (Cyprus). Dark gray areas indicate the inferred locations where rotations occur, at the inside corners of the two ridge-transform intersections (following the model of Allerton, 1989b). Location of spreading axes to the north and south of the transform

DOI:10.1130/G37529.1

faults are unconstrained and shown schematically by dotted lines. B: Outline tectonic map of the Andaman Sea (from Moores et al., 1984). White dashed line encloses a region where ridge segments have similar scale to that proposed for the Troodos spreading system. Gray shading shows late Miocene or younger crust. Ruled area is accretionary prism.

[1]GSA Data Repository item 2016xxx, xxxxxxxx, is available online at www.geosociety.org/pubs/ft2016.htm, or on request from editing@geosociety.org or Documents Secretary, GSA, P.O. Box 9140, Boulder, CO 80301, USA.

Morris and Maffione
Figure 1
Adobe Illustrator CS5, version 15.0.0

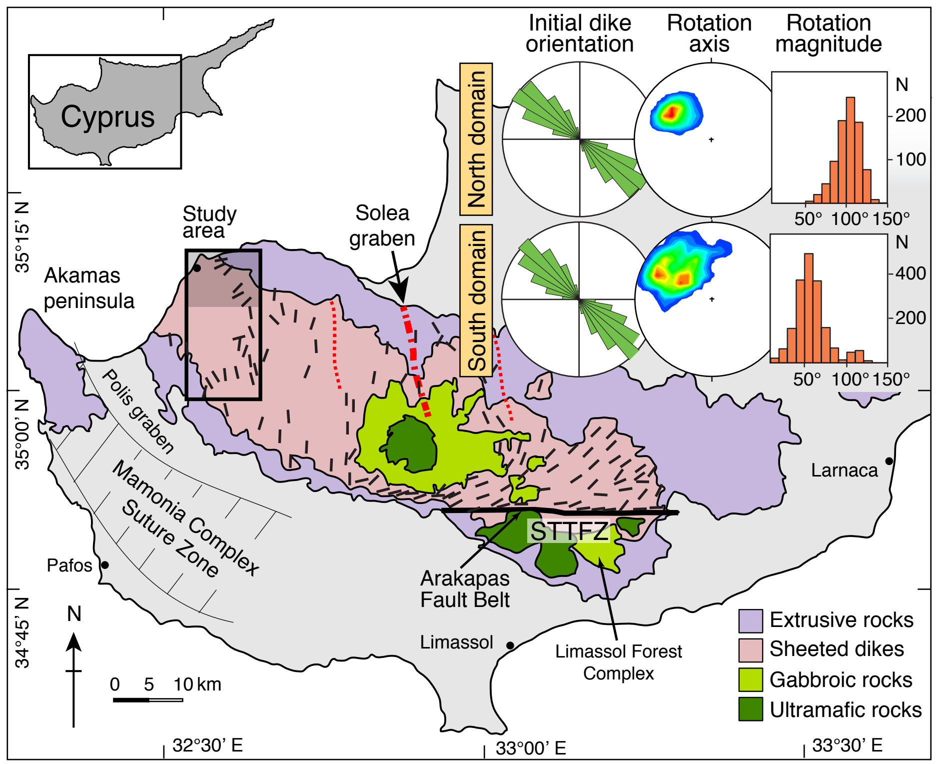

Figure 2 Click here to download Figure G37529_Fig_2_Tectonic_interpretation.pdf

Morris and Maffione
Figure 2
Adobe Illustrator CS5, version 15.0.0

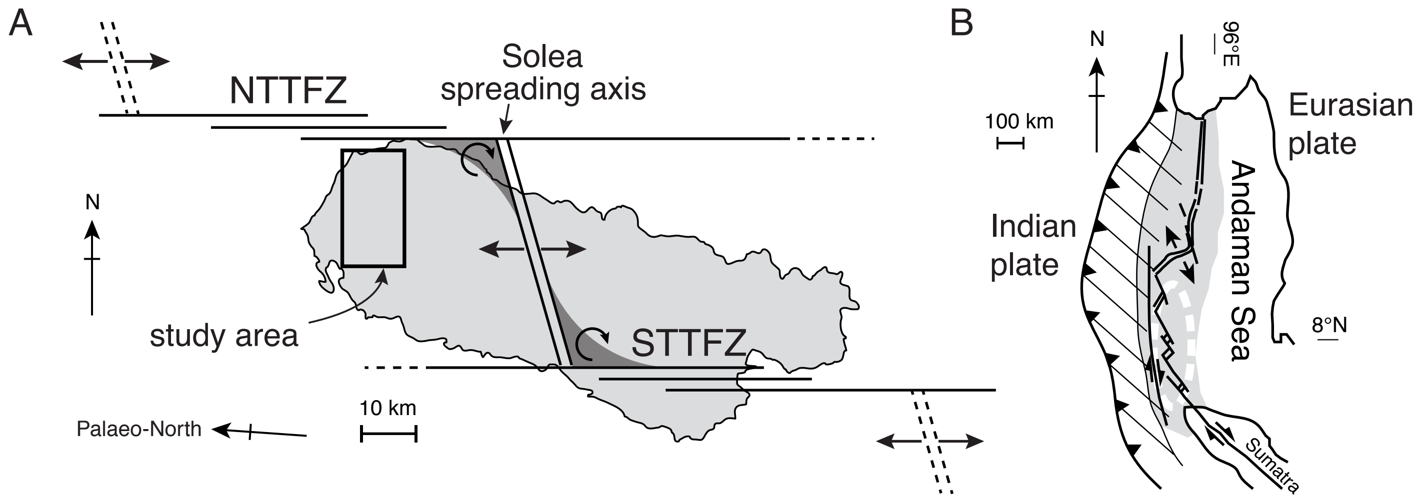

Morris and Maffione
Figure DR1
Adobe Illustrator CS5, version 15.0.0

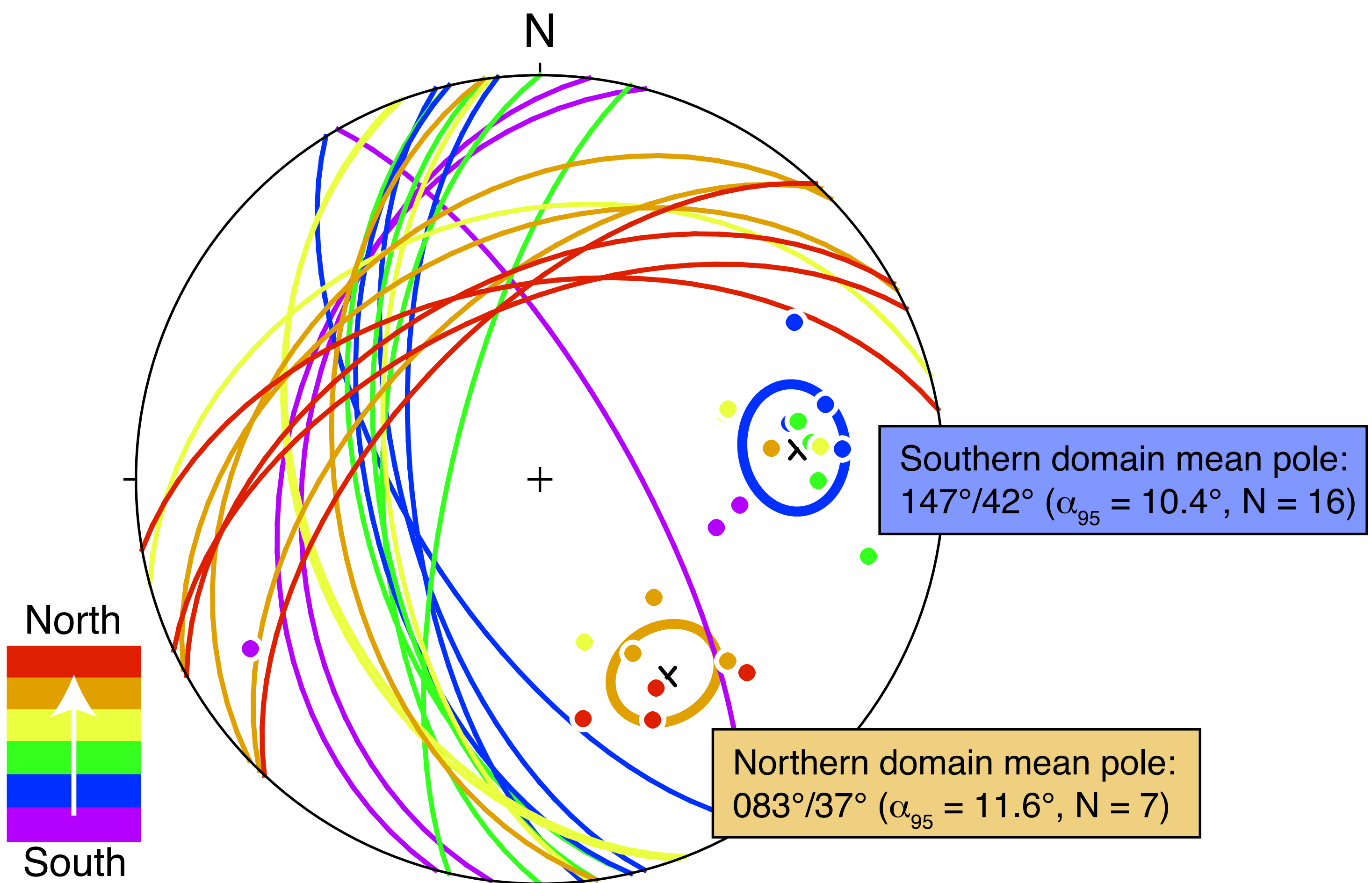

Supplemental Figure 2

Click here to download Supplemental file G37529_Fig_DR2_Paleomagnetic_results.pdf

Morris and Maffione
Figure DR2
Adobe Illustrator CS5, version 15.0.0

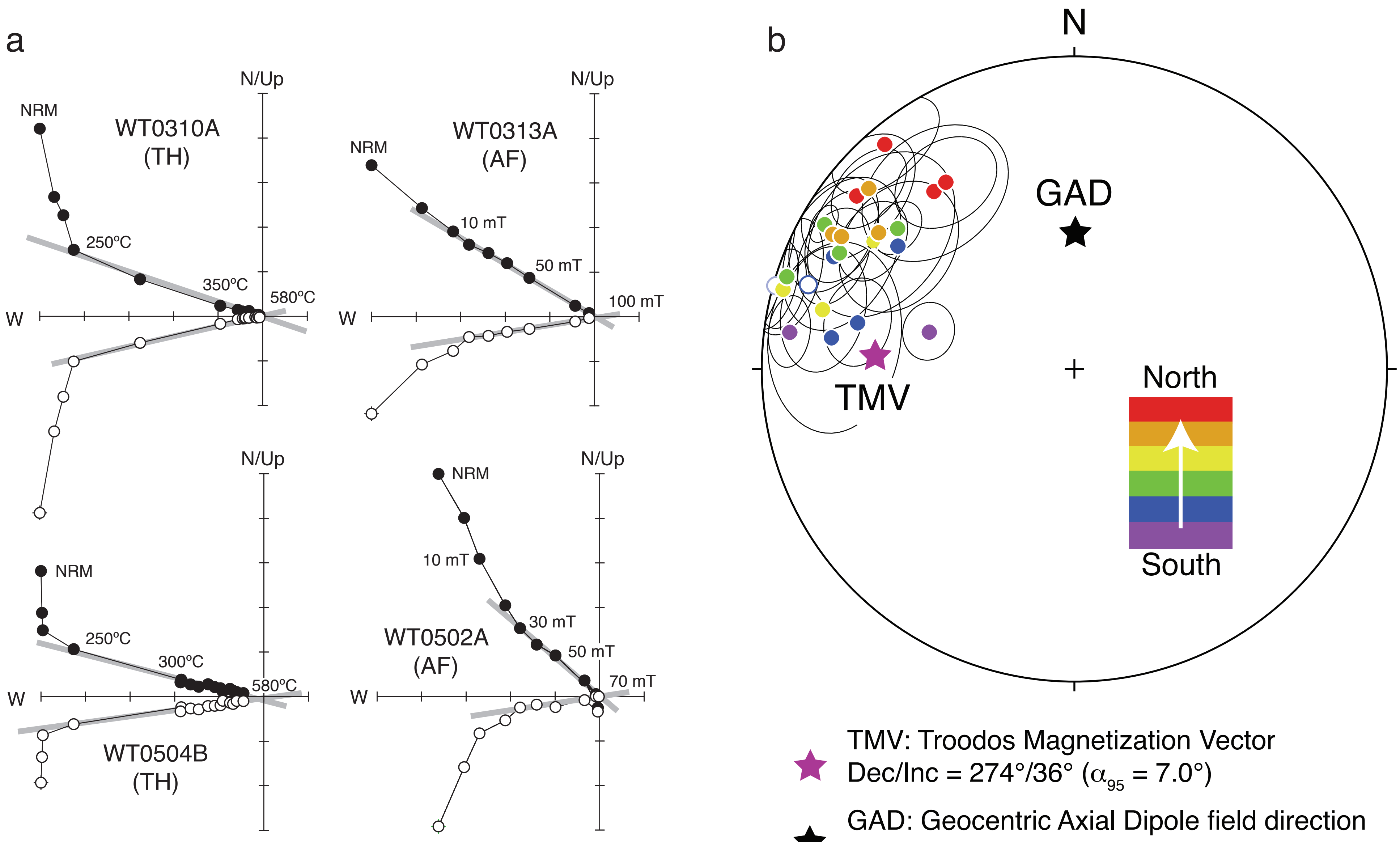

TMV: Troodos Magnetization Vector
Dec/Inc = 274°/36° (α_{95} = 7.0°)

GAD: Geocentric Axial Dipole field direction
Dec/Inc = 000°/54°

Supplemental Figure 3

Click here to download Supplemental file G37529_Fig_DR3_NTR_results.pdf

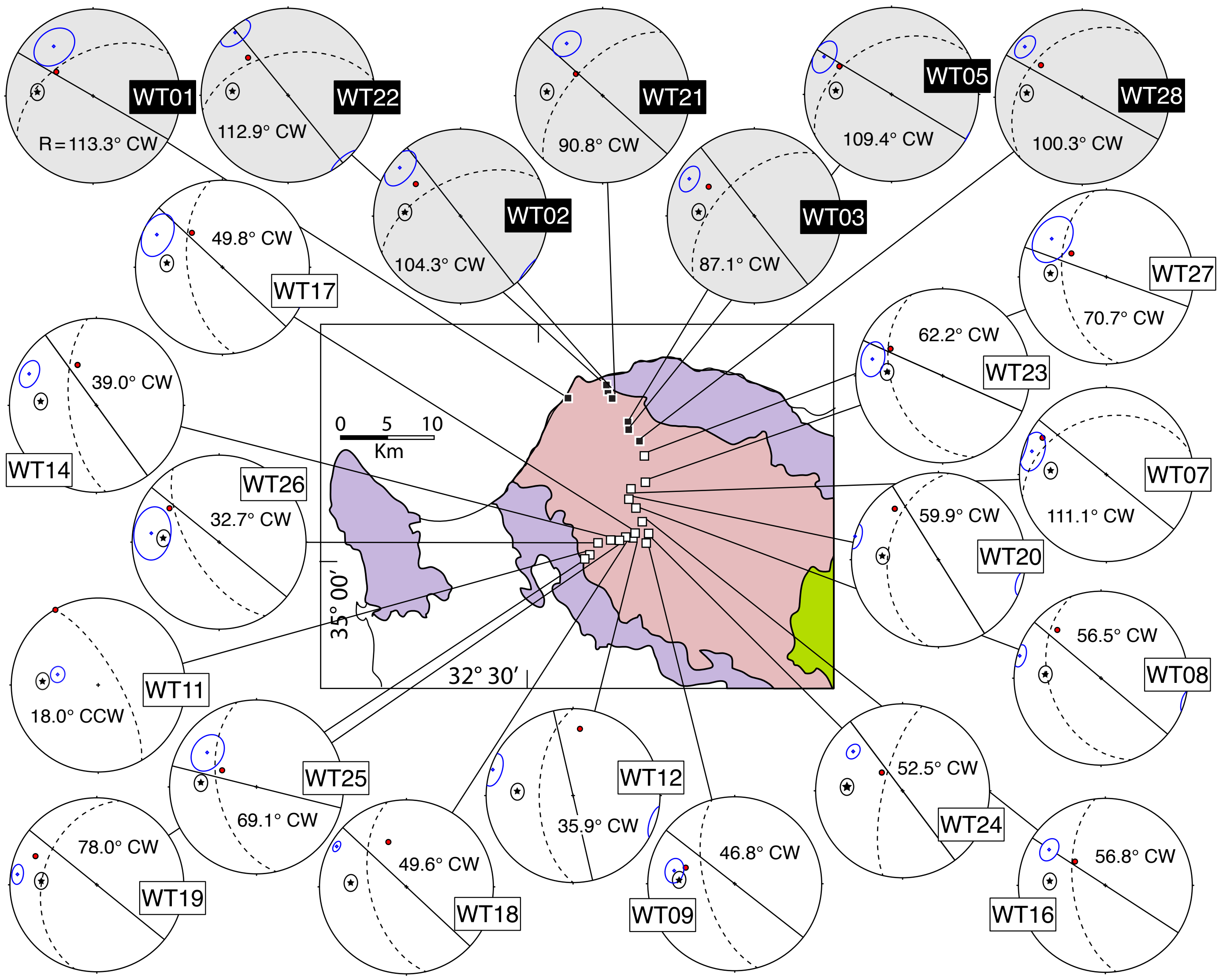

Morris and Maffione
Figure DR3
Adobe Illustrator CS5, version 15.0.0

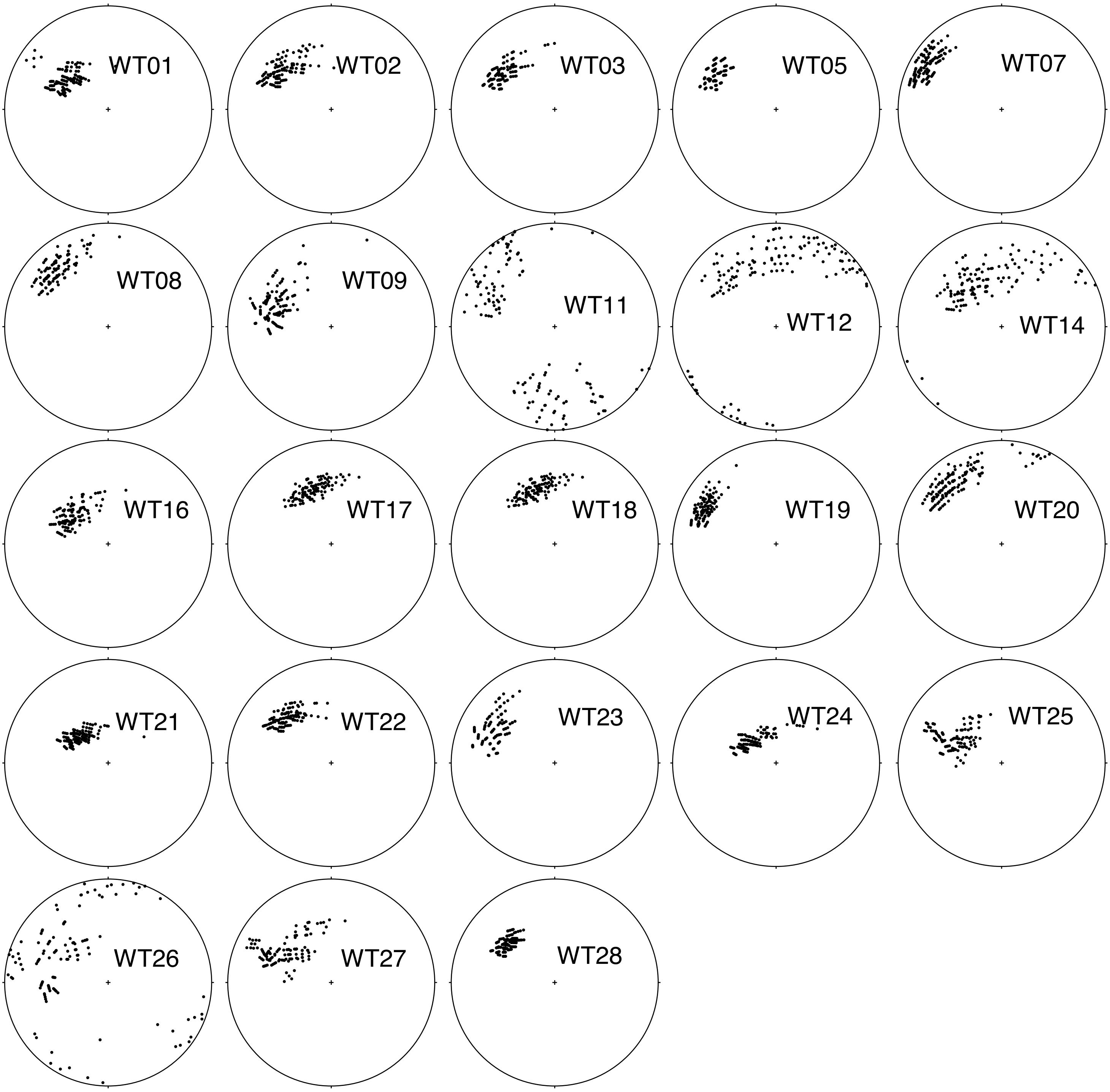

Morris and Maffione
Figure DR4
Adobe Illustrator CS5, version 15.0.0

Supplemental Figure 5

Click here to download Supplemental file G37529_Fig_DR5_Rotation_histograms.pdf

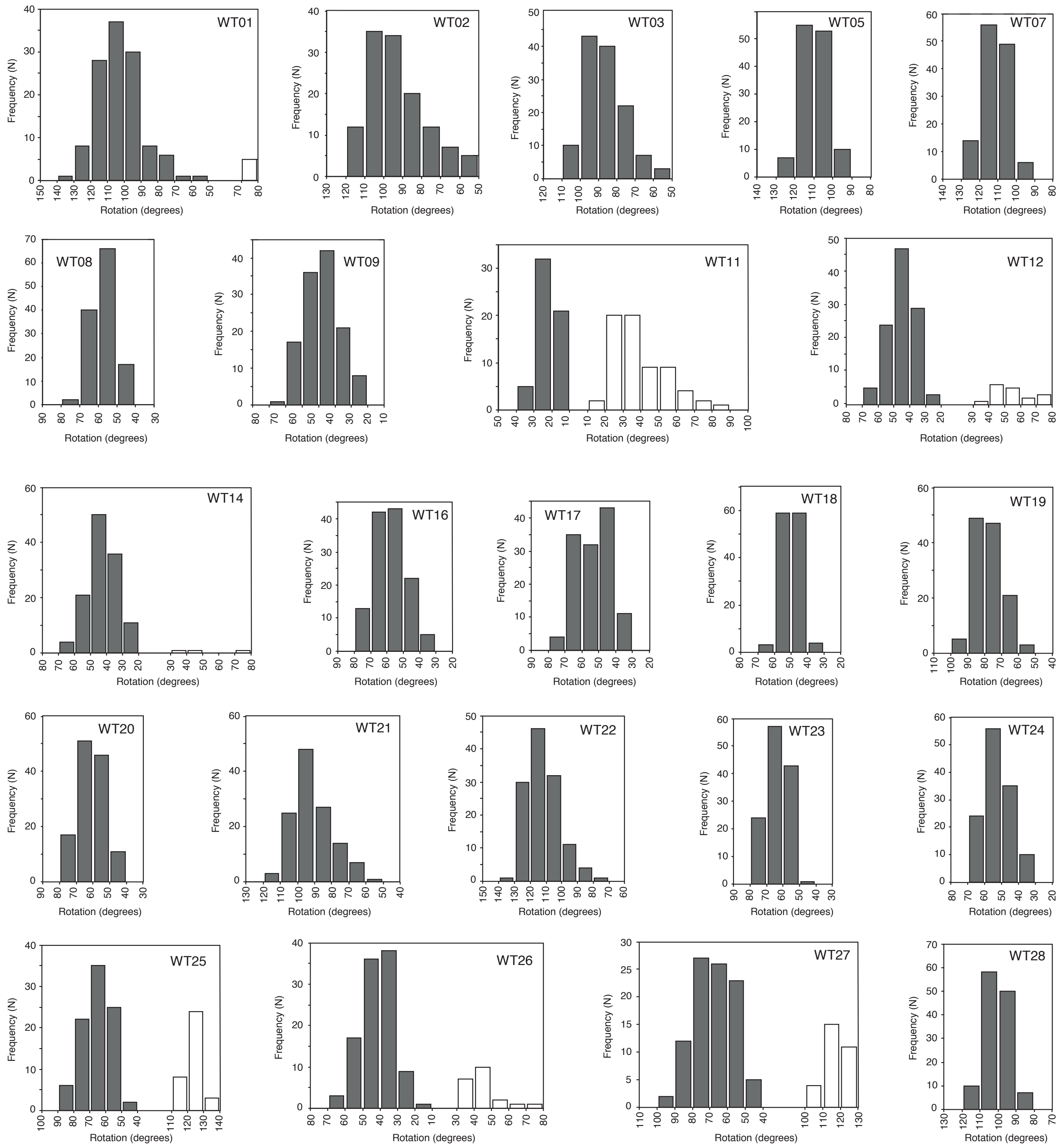

Morris and Maffione
Figure DR5
Adobe Illustrator CS5, version 15.0.0

Data Repository – methods

1.1. Paleomagnetic analysis

Natural remanent magnetizations (NRMs) of samples were investigated via alternating field (AF) demagnetization using an AGICO LDA-3A demagnetizer in 12 incremental steps from 5 to 100 mT. One twin specimen per site was thermally demagnetized with 14-16 temperature increments from 100 to 580°C (or until complete demagnetization) to determine the blocking temperature(s) of the magnetic carriers. Magnetic remanences were measured at each AF or thermal demagnetization step using an AGICO JR-6A spinner magnetometer. Demagnetization data were displayed on orthogonal vector plots (Zijderveld, 1967), and remanence components were isolated via principal component analysis (Kirschvink, 1980) using Remasoft 3.0 software (Chadima and Hrouda, 2006). Site mean directions were evaluated using Fisherian statistics (Fisher, 1953) on virtual geomagnetic poles (VGPs) corresponding to the isolated characteristic remanent magnetizations (ChRMs). All VGPs at each site fell within the 45° cut-off recommended by Johnson et al. (2008). Paleomagnetic quality criteria proposed by Deenen et al. (2011) were adopted to estimate the reliability of the ChRM/VGP distribution at the site level. In particular, the VGP scatter (i.e., A_{95}) obtained at each site was compared to the expected scatter induced by paleosecular variation (PSV) of the geomagnetic field (i.e., A_{95min} - A_{95max}) to assess whether PSV was sufficiently represented in our datasets (Deenen et al., 2011). For values of $A_{95} < A_{95min}$ PSV is not adequately represented, indicating either insufficient time averaging of the geomagnetic field (i.e. sampled dikes were injected in a short period of time), or remagnetization. Conversely, values of $A_{95} > A_{95max}$ may indicate additional (tectonic) processes responsible for the enhanced scatter of paleomagnetic directions.

1.2. Net tectonic rotation

Net tectonic rotation analysis describes the final (net) deformation at a paleomagnetic sampling site in terms of a single rotation about an inclined axis, which, in sheeted dike complexes, simultaneously restores dikes back to their initial (vertical) orientation and their *in situ* mean remanence to an appropriate reference direction. Net tectonic rotation solutions are expressed as the azimuth and plunge of the rotation axis, the magnitude and sense of the rotation, and the initial dike orientation. Key assumptions of this method (Allerton and Vine, 1987) are: (1) remanence was acquired before tilting; (2) an appropriate (coeval) reference magnetization direction may be found; (3) dikes were initially vertical; (4) no significant internal deformation has occurred.

Two solutions are generated if the dike can be restored to the vertical. In this case, additional geological evidence should be used to choose a preferred solution. If a dike cannot be restored to the vertical a single solution is obtained for the rotation axis that restores the dike to its steepest orientation. The uncertainties associated with the calculated net tectonic rotation parameters at each site are directly dependent on the errors associated with the reference magnetization vector, in situ remanence, and dike orientation. To quantify this uncertainty an iterative method was devised by Morris et al. (1998) and successfully applied to the study of the sheeted dikes from other areas of Troodos and other ophiolites. In this method, five potential values (mean value, plus four points located along the 95% ellipses of confidence) are selected for each of the three input vectors used for the analysis. The 125 combinations of input vectors (5 x 5 x 5) provide 125 individual permissible net tectonic rotation solutions at a site (that define an irregular envelope providing a first-order approximation of the 95% confidence region for rotation axes) together with a frequency distribution of associated rotation angles.

References

Allerton, S., and Vine, F. J., 1987, Spreading structure of the Troodos ophiolite, Cyprus: Some paleomagnetic constraints: Geology, v. 15, no. 7, p. 593.

Chadima, M., Hrouda, F., 2006, Remasoft 3.0 a user-friendly paleomagnetic data browser and analyzer. Travaux Géophysiques XXVII, 20–21.

Deenen, M. H. L., Langereis, C. G., van Hinsbergen, D. J. J., and Biggin, A. J., 2011, Geomagnetic secular variation and the statistics of palaeomagnetic directions: Geophysical Journal International, v. 186, no. 2, p. 509-520.

Fisher, R. A., 1953, Dispersion on a sphere: Proc. R. Soc. London, v. 217, p. 295-305.

Johnson, C.L., et al., 2008, Recent investigations of the 0–5 Ma geomagnetic field recorded by lava flows: Geochemistry, Geophysics, Geosystems, v. 9, Q04032, doi.org/10.1029/2007GC001696.

Kirschvink, J. L., 1980, The least-squares line and plane and the analysis of palaeomagnetic data: Geophysical Journal, Royal Astronomical Society, v. 62, no. 3, p. 699-718.

Morris, A., Anderson, M.W., Robertson, A.H.F., 1998, Multiple tectonic rotations and transform tectonism in an intraoceanic suture zone, SW Cyprus: Tectonophysics, v. 299, no. 1-3, p. 229-253.

Zijderveld, J. D. A., 1967, AC demagnetization of rocks: Analysis of results: Methods in Paleomagnetism, p. 254-286.

Figure Captions (Data Repository)

Figure DR1. Equal area stereographic projection (lower hemisphere) of in situ dike orientations within the study area, displayed as planes (great circles) and poles (dots), color-coded by increasing site latitude. Two regions characterized by different dike orientation are recognized: a northern domain with NE-SW-trending dikes, and a southern domain with mainly N-S-trending dikes. Cones of 95% confidence around the dike poles calculated separately for the northern and southern domain demonstrate statistically significant differences (~60°) between the mean dike orientations in the two domains. Three sites in late dikes (see text) and two additional sites showing inconsistent dike orientations, have been excluded from the computation of mean dike orientations.

Figure DR2. (a) Representative orthogonal vector plots (in situ coordinates) for twin specimens demagnetized thermally (TH) and using alternating fields (AF). Solid/open circles are projections of the remanence vector onto the horizontal/vertical planes respectively. Demagnetization steps are in °C or millitesla (mT). Gray lines are the characteristic remanent magnetizations (ChRMs) isolated in each specimen. (b) Equal area stereographic projection (lower hemisphere) of site mean directions (dots) and associated α_{95} cones of confidence (gray ellipses) from all sites sampled, color-coded by increasing site latitude. Colored/open symbols represent positive/negative inclinations respectively. Purple star, Troodos magnetization vector (TMV; declination/inclination = 274°/36°, α_{95} = 7.0°; Clube and Robertson (1985)). Black star, direction of the present geocentric axial dipole field (GAD) in Cyprus (D/I = 000°/54.6°).

Figure DR3. Equal area stereographic projections showing results of net tectonic rotation analysis at all sampled sites. Gray/white projections and black/white squares on the geological map indicate sites in the northern/southern domains, respectively (see text); black stars, Troodos reference direction (TMV); blue dots, *in situ* site mean remanence directions (with associated 95% cones of confidence); red dots, net tectonic rotation axes; R, amount of rotation (CW, clockwise; CCW, counterclockwise).

Figure DR4. Equal area stereographic projections showing the 125 permissible rotation axes (black dots) computed by net tectonic rotation analysis at each sampling site. The scatter of the permissible rotation axes provides a first-order estimate of the error associated with the mean rotation axis calculated at each site.

Figure DR5. Histograms of the 125 permissible rotation magnitudes obtained at each site. Dark gray and white bars indicate CW and CCW net rotation, respectively.

Table DR1. Paleomagnetic results from the sheeted dike complex of the western Troodos ophiolite.^{D} Discrete dike. Dike orientation is expressed as strike/dip. $DP\alpha_{95}$, 95% cone of confidence around the calculated mean dike orientation. D, I, declination and inclination of *in situ* site mean remanence. dD, dI, declination and inclination error, respectively. k, α_{95}, precision parameter and 95% cone of confidence around the site mean characteristic remanent magnetizations (ChRMs) after Fisher (1955). K, A_{95}, precision parameter and 95% cone of confidence around the site mean virtual geomagnetic pole (VGP). A_{95min}, A_{95max}, minimum and maximum value of A_{95}

expected from paleosecular variation (PSV) of the geomagnetic field, according to Deenen et al. (2011). N, number of total samples used for the statistics.

Table DR2. Results of net tectonic rotation analysis in the sheeted dike complex of the western Troodos ophiolite. Sites are listed in geographical order from north to south. Both preferred (gray area) and alternate solutions are reported. For each solution the azimuth (Az) and plunge of the rotation axis, the rotation angle (R) and sense of rotation, and the initial dike strike and dip are listed. *, discarded sites (see text).

Table DR1. Paleomagnetic results from the sheeted dike complex of the western Troodos ophiolite.

Site	Latitude (°N)	Longitude (°E)	Dyke str./dip	DP α_{95}	Mean remanence vector D	dD	I	dI	k	α_{95}	K	A_{95}	A_{95min}	A_{95max}	N
WT01	35°09'26.43"	32°32'32.08"	241/49	9.3	321.6	18.4	28.0	29.6	12.2	18.0	12.5	17.7	5.5	24.1	7
WT02	35°10'10.18"	32°35'29.97"	245/55	7.6	308.5	10.1	11.6	19.5	15.2	14.7	31.3	10.1	5.2	22.1	8
WT03	35°07'51.51"	32°36'51.82"	224/54	4.0	299.7	7.9	15.0	14.9	23.1	10.3	39.0	7.8	4.8	19.2	10
WT04[D]	35°07'51.51"	32°36'51.82"	149/44	9.9	291.9	8.2	22.7	14.2	39.4	9.7	57.9	8.0	5.5	24.1	7
WT05	35°07'34.37"	32°36'50.88"	242/40	3.6	299.2	12.0	12.1	23.2	20.3	12.6	22.3	12.0	5.2	22.1	8
WT06[D]	35°07'34.37"	32°36'50.88"	140/59	8.4	295.4	6.3	20.4	11.2	50.6	7.9	81.2	6.2	5.2	22.1	8
WT07	35°04'20.64"	32°37'0.476"	255/34	8.2	287.7	9.7	-11.3	18.7	15.7	14.4	34.2	9.6	5.2	22.1	8
WT08	35°03'18.11"	32°37'20.47"	160/40	7.8	285.4	5.2	3.4	10.3	53.0	7.7	115.6	5.2	5.2	22.1	8
WT09	35°01'19.87"	32°37'59.21"	165/62	8.9	282.2	7.7	29.5	12.2	31.5	10.0	56.4	7.4	5.2	22.1	8
WT10[D]	35°01'19.87"	32°37'59.21"	035/80	5.0	291.2	6.2	26.9	10.2	52.2	7.7	84.8	6.0	5.2	22.1	8
WT11	35°00'34.41"	32°34'07.45"	330/72	8.9	284.5	9.2	50.1	8.8	62.6	7.1	49.8	7.9	5.2	22.1	8
WT12	35°01'39.39"	32°37'08.49"	180/58	9.3	287.9	9.3	3.4	18.6	24.5	11.4	36.1	9.3	5.2	22.1	8
WT13 [D]	35°01'39.39"	32°37'08.49"	143/75	5.0	294.1	6.0	15.5	11.2	61.8	7.7	104.9	5.9	5.5	24.1	7
WT14	35°01'29.88"	32°35'38.05"	174/64	9.5	295.1	8.1	15.7	15.2	28.5	10.6	48.4	8.0	5.2	22.1	8
WT15 [D]	35°01'29.88"	32°35'38.05"	200/41	7.8	292.6	4.7	9.9	9.2	56.2	7.5	140.2	4.7	5.2	22.1	8
WT16	35°02'32.22"	32°37'45.26"	173/59	8.7	302.4	9.5	24.4	16.1	52.0	9.4	53.5	9.2	5.9	26.5	6
WT17	35°01'46.97"	32°37'15.32"	172/57	4.5	296.4	14.1	16.9	26.1	21.2	17.0	31.1	13.9	6.3	29.7	5
WT18	35°01'41.99"	32°36'40.10"	167/55	6.4	300.1	3.4	8.1	6.7	188.9	4.0	263.5	3.4	5.2	22.1	8
WT19	35°00'24.65"	32°33'55.04"	195/37	10.4	277.5	4.7	8.7	9.1	61.1	7.1	142.9	4.7	5.2	22.1	8
WT20	35°00'24.65"	32°33'55.04"	187/41	7.2	285.7	5.7	-0.5	11.5	65.3	8.4	137.1	5.7	5.9	26.5	6
WT21	35°09'37.42"	32°35'37.56"	223/59	5.3	325.4	12.0	27.9	19.4	21.2	12.3	23.9	11.6	5.2	22.1	8
WT22	35°09'57.33"	32°35'30.63"	260/50	6.2	319.8	7.5	6.2	14.8	21.2	12.3	55.7	7.5	5.2	22.1	8
WT23	35°04'55.15"	32°37'55.68"	159/41	3.4	283.4	11.9	18.0	21.7	18.1	13.4	23.3	11.7	5.2	22.1	8
WT24	35°01'55.13"	32°38'09.95"	193/72	2.1	308.5	5.8	28.2	9.3	73.7	6.5	99.9	5.6	5.2	22.1	8
WT25	35°01'26.85"	32°36'15.08"	167/53	6.4	304.9	17.2	31.4	26.2	12.9	16.0	12.3	16.4	5.2	22.1	8
WT26	35°01'19.63"	32°34'45.69"	148/63	8.5	277.5	20.6	22.4	35.9	14.5	20.8	15.4	20.1	6.3	29.7	5
WT27	35°06'07.11"	32°37'53.82"	172/48	9.4	304.9	14.0	24.3	23.9	12.4	19.8	24.9	13.7	5.9	26.5	6
WT28	35°06'55.81"	32°37'33.77"	226/33	5.9	311.3	7.9	13.1	15.0	34.9	9.5	51.3	7.8	5.2	22.1	8

Table DR2. Net tectonic rotation solutions for sheeted dikes of the western Troodos ophiolite.

Site	Preferred solution						Alternate solution					
	Rotation axis		R	Sense	Initial dike		Rotation axis		R	Sense	Initial dike	
	Az	Plunge			Strike	Dip	Az	Plunge			Strike	Dip
Northern domain												
WT02	305.6	36.8	104.3	CW	322	90	069.9	30.5	42.1	CW	046	90
WT22	313.2	37.0	112.9	CW	321	90	070.7	39	52.6	CW	047	90
WT21	309.2	57.4	90.8	CW	312	90	113.8	4.1	64.8	CW	056	90
WT01	303.2	48.1	113.3	CW	300	90	110.7	8.4	56.7	CW	068	90
WT03	302.6	37.7	87.1	CW	322	90	079.1	8.4	43.3	CW	046	90
WT05	298.3	32.4	109.4	CW	301	90	081.3	2.6	51.9	CW	067	90
WT28	307.8	39.7	100.3	CW	299	90	096.0	02	68.0	CW	069	90
Southern domain												
WT27	303.9	49.9	70.7	CW	290	90	284.9	19.3	99.1	CCW	078	90
WT23	297.4	32.9	62.2	CW	294	90	269.9	23.2	97.6	CCW	074	90
WT07	299.9	16.4	111.1	CW	309	90	049.2	4.5	58.4	CW	060	90
WT20	319.4	23.9	59.9	CW	328	90	249.4	6.7	65.8	CCW	049	90
WT08	317.8	26.1	56.5	CW	310	90	263.6	13.9	93.0	CCW	058	90
WT16	308.1	53.5	56.8	CW	303	90	283.4	19.7	96.6	CCW	065	90
WT24	311.3	64.0	52.5	CW	323	90	286.4	13	73.9	CCW	045	90
WT17	318.4	46.1	49.8	CW	313	90	276.1	16.6	91.3	CCW	056	90
WT18	338.1	43.7	49.6	CW	313	90	275.8	11.8	100.0	CCW	055	90
WT12*	005.9	23.9	35.9	CW	347	90	249.3	4.9	57.8	CCW	021	90
WT14*	335.0	47.5	39.0	CW	324	90	273.7	15.4	85.4	CCW	044	90
WT25	295.8	53.8	69.1	CW	284	90	287.9	24.7	105.6	CCW	084	90
WT09	288.2	40.4	46.8	CW	308	90	274.6	29.4	91.2	CCW	060	90
WT26*	304.3	31.5	32.7	CW	309	90	270.1	27.9	106.4	CCW	059	90
WT11*	330.3	0.6	18.0	CCW	330	90	285.6	40.1	106.5	CCW	038	90
WT19	295.0	23.2	78.0	CW	309	90	252.8	18.2	66.2	CCW	059	90